Isr. J. Earth Sci. 1989; 38:1–17

# Pressures and temperatures of Pan-African high-grade metamorphism in the Elat Association, NE Sinai

**Alan Matthews, Arthur P.S. Reymer*, Dov Avigad, Joshua Cochin, and Shmuel Marco**

Department of Geology, Institute of Earth Sciences, The Hebrew University of Jerusalem, Jerusalem 91904, Israel

*(Received 27 January 1989 and in revised form 3 May 1989)*

## ABSTRACT

**Matthews, A., Reymer, A.P.S., Avigad, D., Cochin, J., Marco, S. 1989. Pressures and temperatures of Pan-African high-grade metamorphism in the Elat Association, NE Sinai. Isr. J. Earth Sci. 38:1–17.**

Continuous reaction exchange geothermobarometry (Mg/Fe between garnet and biotite; Ca between garnet and plagioclase) has been applied to pressure and temperature determination in garnet and staurolite-cordierite-$Al_2SiO_5$ grade pelitic metamorphic zones of the Campus area of the Precambrian Elat Association.

Electron microprobe analysis of the chemical compositions of rims of coexisting minerals in both zones are well distributed on AFM projections and appear to demonstrate equilibrium parageneses. Biotites and plagioclases, respectively, show little evidence of chemical zonation with respect to $MgFe^{-1}$ and Ca, which is consistent with their high modal abundance, whereas garnets in staurolite-cordierite-$Al_2SiO_5$ grade assemblages show systematic zoning profiles with $MgFe^{-1}$ and $X$.Ca decreasing from cores to rims. Translating the various fractionations into temperatures and pressures gives conditions of 604 ± 26°C; 4.60 ± 0.80 kbar for garnet cores and 583 ± 25°C; 3.84 ± 0.69 kbar for garnet rims. These are taken to represent a peak and slightly post-peak segment of the metamorphic $P$–$T$ path. Garnet-zone samples give temperatures in the range 580–660°C. These temperatures are anomalously high for typical "garnet zone" conditions, and possibly represent thermal effects associated with the intrusion of the adjacent granite (gneiss) which were not eradicated during subsequent metamorphism and deformation.

Regional heat flow associated with large-scale magmatic activity and direct advection of heat into rocks through intrusion contributed to the heat sources of Pan-African metamorphism in Sinai.

## INTRODUCTION

The metamorphic–igneous rock complex of the Elat area, S Israel, is one of several late-Precambrian (Pan-African) orogenic complexes dispersed within the granitic igneous basement of the Arabian–Nubian massif in Sinai (Fig. 1a).

In their present configuration the rocks of the orogenic complex in the Elat area are broken up into several different blocks which formed as a result of tectonic displacements associated with the Dead Sea transform. Garfunkel (1980) grouped the rocks into two associations, the Elat and Roded (Fig. 1b). The present study focuses on the temperature and pressure conditions in high-grade metamorphic rocks of the Campus area of the Elat Association (Fig. 1c).

The structural, metamorphic, and igneous evolu-

* Present address: TNO-TPD, Department of Ceramics, Technical University, 5600 MB Eindhoven, The Netherlands.



0021-2164/89$4.00

tion of the Elat Association has been the subject of a number of studies including those of Bentor (1961), Garfunkel (1970, 1980), Page (1972), Shimron (1972), Eyal (1975), Avigad (1984), Reymer et al. (1984a), and Avigad and Matthews (1985). The structural and metamorphic evolution of the probable extension of the Elat Association to the south in the area between Wadi Twaiba and Wadi Um Mara has been discussed in detail by Eyal (1975, 1980). The igneous and metamorphic history evidenced in the Campus area (Fig. 1c) is generally considered to have commenced with the intrusion of micaceous metasediments by basic gabbroic to dioritic rocks followed by granites. Metamorphism and deformation resulted in the formation of a sequence of medium-to-high-grade metasediments, amphibolites, and granite gneisses. Cessation or waning of this phase of deformation and metamorphism was followed by the intrusion of swarms of dikes of basic to intermediate composition which, together with all the older metamorphic rocks, underwent a lat-

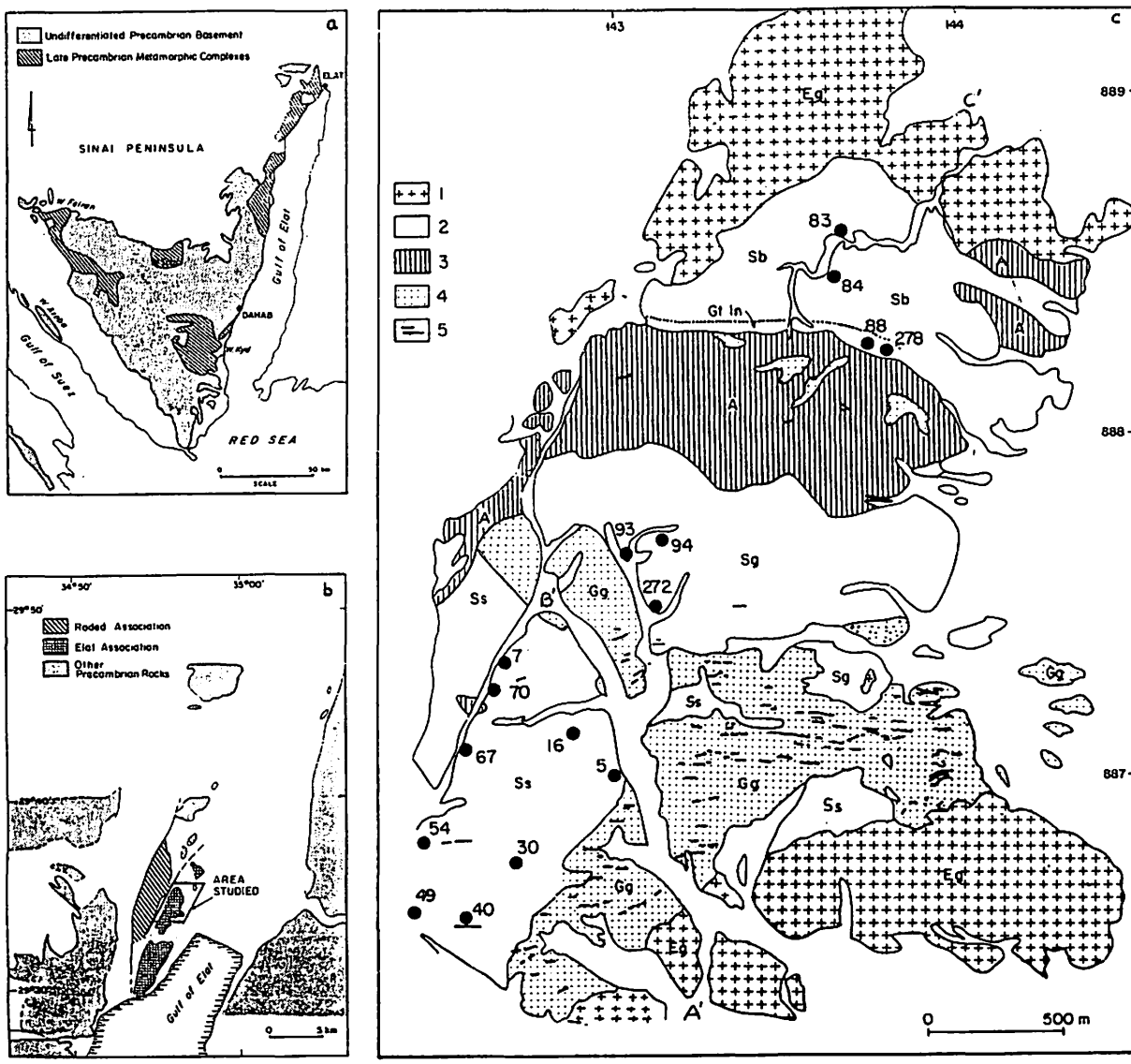


Fig. 1. Geological setting of the Elat metamorphic rocks.
a — Map showing distribution of metamorphic complexes in Sinai (after Shimron, 1972).
b — Map showing location of the Elat and Roded metamorphic associations in the Elat area (after Garfunkel, 1980).
c — Geological map of the Campus area of the Elat Association (modified after Shimron, 1972). Sample location sites are indicated by numbers. Legend: (1) Elat granite (Eg); (2) Micaceous metasediments: Sb = biotite zone, Sg = garnet zone; Ss = staurolite-cordierite-$Al_2SiO_5$ zone; (3) Amphibolites (A); (4) Granite gneiss (Gg); (5) Metamorphosed dikes. "Gt In" (dotted line) indicates the approximate boundary at which garnet appears in the schists.

er upper greenschist facies metamorphic overprint and further deformation. The cycle of metamorphic–plutonic igneous events was completed by the intrusion of the calc-alkaline Elat granite (Fig. 1c). Age relations constrained by Rb–Sr studies (Bielski, 1982; Halpern, 1980; Halpern and Tristan, 1982) placed deposition of shaly sediment protoliths at 800 ± 43 Ma, the main phase of metamorphism probably at around 650 Ma, and intrusion of the Elat granite at around 600 Ma.

The metasedimentary sequence in the Campus area varies in grade from pelitic biotite zone through garnet zone to high-grade staurolite-cordierite-$Al_2SiO_5$-bearing rocks (Fig. 1c) and is of the lower-pressure andalusite-sillimanite type, a characteristic shared with the other metamorphic complexes of Sinai, such as the Wadi Kid complex and Ataqa wedge of SE Sinai (Shimron, 1980, 1987; Reymer, 1983; Reymer et al., 1984b; Beyth et al., 1987). In such areas the nature of the heat sources becomes a dominant question: to what extent do the high-grade, low-pressure, metamorphic conditions represent an ambient regional heat flow in sequences of buried sediments and volcanics, or in what way are local igneous phenomena contributing to the thermal budget.

The answers to such questions lie in part in the development of a detailed knowledge of the pressure and temperature ($P$–$T$) conditions of metamorphism. In this respect one of the major advances in metamorphic petrology in recent years has been the development of self-consistent thermodynamic data sets and accurate activity models which can be applied to continuous reaction thermobarometry (e.g., Holland and Powell, 1985; Powell and Holland, 1988). In a preliminary study of the $P$–$T$ conditions in the Wadi Kid Complex, Reymer et al. (1984b) used continuous reaction thermobarometry to determine temperatures and pressures for staurolite-$Al_2SiO_5$-bearing rocks and anatectic K-feldspar-bearing gneisses. We report here the results of a mineral chemistry and geothermobarometry study on the staurolite-cordierite-$Al_2SiO_5$-bearing rocks in the SW of the Campus area and on the garnet zone rocks to the north (Fig. 1c), and we explore the relevance of the results for the interpretation of the thermal evolution of Pan-African metamorphism in Sinai.

## GEOLOGICAL SETTING

The Elat Association in the Campus area is composed of five major rock groups: micaceous metasediments; amphibolites; granite gneisses; metamorphosed dikes, and the calc-alkaline Elat granite (Fig. 1c). Detailed mapping and mineralogical studies in the area by Shimron (1972) resulted in the definition of four zones in pelitic rocks: biotite, garnet, staurolite-andalusite, and cordierite. The highest-grade cordierite-bearing rocks were considered to represent the zenith of a thermal dome with temperatures progressively decreasing down to the lowest-grade biotite zone assemblages. Four phases of folding were identified, of which the first two were primarily associated with the development of high-grade mineralogies. The first phase (F1), with axes trending approximately E–W, leads to the formation of isoclinal folds and a well-defined regional schistosity. The second phase (F2) also trends E–W, and consists of open-to-tight folds with a near-vertical, non-penetrative cleavage. A particularly well-defined F2 synform structure relates the granite gneiss and overlying staurolite-cordierite-$Al_2SiO_5$-bearing rocks in the SW of the Campus area (Garfunkel, 1980). Shimron (1972) considered that the highest grades of metamorphism, the intrusion of the granite gneiss and its foliation development, were broadly coeval, primarily occurring before, during, and in the immediate aftermath of the F2 folding phase.

Garfunkel (1980) and Avigad (1984) placed the intrusion of the mafic dikes after the second-phase folding of the contact between granite gneiss and the high-grade schists. Metamorphism in the upper greenschist facies and the development of schistosity in these dikes as a result of later deformation phases thus occurred during the cooling and uplifting of the complex. The imprint of this overprint on the high-grade metamorphic assemblages is generally confined to the retrogression of high-grade iron-bearing minerals, such as cordierite, to chlorite.

The regional cleavage (S1) which occurs in all major rock types (apart from the metamorphosed dikes and the Elat granite), dips to the south outside the F2 synform, with a corresponding alignment of lithological boundaries. This, combined with the fact that granite gneisses enclose staurolite-cordierite-$Al_2SiO_5$-zone rocks in the F2 synform, lead Reymer et al. (1984a) (summarized in Avigad and Matthews, 1985) to conclude that the metamorphic sequence is inverted, with lower-grade (biotite, garnet zone) rocks apparently being progressively overlain by sequences of higher-grade rocks. These features were interpreted as the result of the development of a large-scale overturned fold (Fig. 2).

The granite gneiss always separates garnet-zone rocks from staurolite-cordierite-$Al_2SiO_5$-bearing rocks; furthermore, whereas the contact between the granite gneiss and the garnet zone clearly has an intrusive

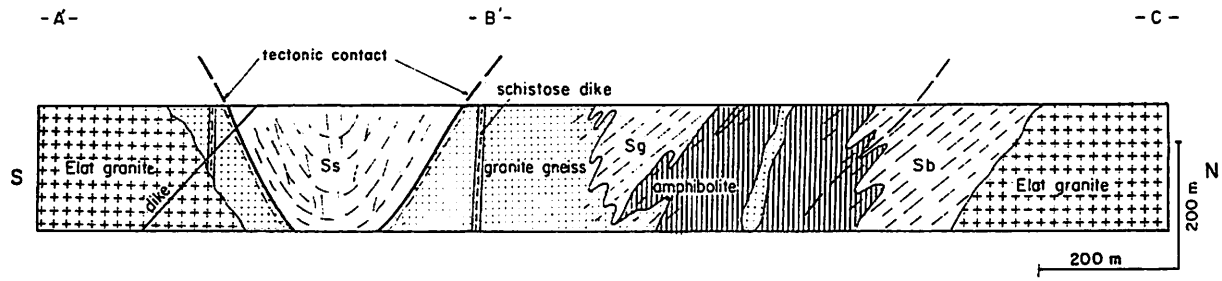


Fig. 2. Schematic cross-section of the Campus area of the Elat Association, illustrating the model of structural evolution suggested by Reymer et al. (1984a). Cross-section corresponds to the lines joining points A' B' C' in Fig. 1c. Diagram modified after Avigad and Matthews (1985).

character, that between the staurolite-cordierite-$Al_2SiO_5$-bearing rocks appears in many places to have a tectonic character.

The regional scheme suggested by Reymer et al. (1984a) and Avigad and Matthews (1985) is illustrated in Fig. 2. It views a buried metamorphic sequence consisting of pelites/basic rocks/granites (intrusive into the garnet-zone pelites and basic rocks) being overturned and inverted during the first folding phase; any thrusting of staurolite-cordierite-$Al_2SiO_5$ grade rocks on top of the granite gneisses may have been contemporary with this folding and the sequence in the SW of the complex was folded into a syncline by the second phase.

In this study the differentiation of high-grade pelitic rocks into separate staurolite-$Al_2SiO_5$ and cordierite zones is not made; instead the rocks are grouped together in a single zone.

## MINERAL ANALYSIS AND PETROGRAPHY

The samples were taken from the biotite zone, from the garnet zone north of the amphibolite body and near the southern contact with the granite gneisses, and from the staurolite-cordierite-$Al_2SiO_5$ zone overlying the granite gneisses in the large F2 synform to the SW of the area. The locations of the analyzed samples, which were selected on the basis of freshness and absence of metamorphic retrogradation, are given in Fig. 1c. Mineral assemblages are detailed in Table 1. Electron microprobe analyses were made on the following minerals: biotite zone — biotites; garnet zone — garnets + biotites; and staurolite-cordierite-$Al_2SiO_5$ zone — garnets-biotites-plagioclase ± staurolite ± cordierite. Details of analytical procedures may be found in Reymer et al. (1984b). Of the minerals analyzed, only the garnets were found to show any significant zonation, and for these, separate core and rim chemical analyses were made. All other analyses were on the rims of minerals. The choice of mineral grains for analyses was made using the criterion that all grains show mutual contact relationships in the specimen area.

Electron microprobe analyses of minerals from the garnet and biotite zones are presented in Table 2, and from the staurolite-cordierite-$Al_2SiO_5$ zone, in Table 3.

Table 1. Mineral assemblages of analyzed samples

| | Garnet zone | | | | Staurolite-cordierite-$Al_2SiO_5$ zone | | | | | | | | |
|---|---|---|---|---|---|---|---|---|---|---|---|---|---|
| Sample # | 88 | 94 | 272 | 93 | 7 | 70 | 67 | 54 | 5 | 49 | 16 | 30 | 40 |
| Minerals | | | | | | | | | | | | | |
| Quartz | x | x | x | x | x | x | x | x | x | x | x | x | x |
| Plagioclase | x | x | x | x | • | • | • | • | • | • | • | • | • |
| Biotite | • | • | • | • | • | • | • | • | • | • | • | • | • |
| Garnet | • | • | • | • | • | • | • | • | • | • | • | • | • |
| Muscovite | | | | | x | | | x | x | x | x | x | x |
| Chlorite | | | | | x | | x | | x | x | | x | |
| Andalusite | | | | | x | | | | | | | x | x |
| Sillimanite | | | | | x | | | | x | x | | x | x |
| Staurolite | | | | | • | • | • | x | x | • | x | x | • |
| Cordierite | | | | | | | • | | | | | | |

Minerals shown by a dot were analyzed by electron microprobe; those indicated by an x were present in the assemblages but were not analyzed.

Table 2. Electron microprobe analyses of minerals from the biotite and garnet zones, Campus area, Elat Association

| Sample# | 83* | | 84* | | 278 | | 88 | | 88 | | 94 | | 94 | | 272 | | 272 | | 93 | | 93 | | 93 | |
|---|---|---|---|---|---|---|---|---|---|---|---|---|---|---|---|---|---|---|---|---|---|---|---|---|
| | Wt% | Cat. | Wt% | Cat. | Wt% | Cat. | Wt% | Cat. | Wt% | Cat. | Wt% | Cat. | W% | Cat. | Wt% | Cat. | Wt% | Cat. | Wt% | Cat. | Wt% | Cat. | Wt% | Cat. |
| *Biotites* | | | | | | | | | | | | | | | | | | | | | | | | |
| $SiO_2$ | 35.84 | 2.790 | 34.64 | 2.702 | 34.71 | 2.691 | 34.21 | 2.655 | | | 34.01 | 2.683 | | | 39.90 | 2.649 | | | 33.43 | 2.636 | 33.43 | 2.636 | | |
| $Al_2O_3$ | 15.95 | 1.464 | 17.43 | 1.603 | 18.56 | 1.696 | 19.15 | 1.752 | | | 19.24 | 1.790 | | | 18.48 | 1.702 | | | 18.05 | 1.678 | 18.05 | 1.678 | | |
| FeO | 19.16 | 1.247 | 19.84 | 1.294 | 20.45 | 1.326 | 20.07 | 1.303 | | | 21.58 | 1.424 | | | 22.44 | 1.466 | | | 23.11 | 1.524 | 23.11 | 1.524 | | |
| $Fe_2O_3$ | 0.00 | 0.00 | 0.00 | 0.00 | 0.00 | 0.00 | 0.00 | 0.00 | | | 0.00 | 0.00 | | | 0.00 | 0.00 | | | 0.00 | 0.00 | 0.00 | 0.00 | | |
| MgO | 10.35 | 1.201 | 9.88 | 1.149 | 9.32 | 1.077 | 8.96 | 1.036 | | | 8.48 | 0.997 | | | 8.31 | 0.968 | | | 8.29 | 0.974 | 8.29 | 0.974 | | |
| MnO | 0.00 | 0.00 | 0.00 | 0.00 | 0.13 | 0.009 | 0.23 | 0.015 | | | 0.12 | 0.008 | | | 0.27 | 0.018 | | | 0.19 | 0.013 | 0.19 | 0.013 | | |
| $TiO_2$ | 2.51 | 0.147 | 2.51 | 0.147 | 1.37 | 0.080 | 1.62 | 0.095 | | | 1.01 | 0.060 | | | 1.69 | 0.099 | | | 1.60 | 0.095 | 1.60 | 0.095 | | |
| $Na_2O$ | 0.09 | 0.014 | 0.09 | 0.014 | 0.19 | 0.029 | 0.34 | 0.051 | | | 0.16 | 0.024 | | | 0.00 | 0.00 | | | 0.00 | 0.024 | 0.00 | 0.024 | | |
| CaO | 0.03 | 0.003 | 0.05 | 0.004 | 0.04 | 0.003 | 0.10 | 1.008 | | | 0.14 | 0.012 | | | 0.04 | 0.003 | | | 0.22 | 0.019 | 0.22 | 0.019 | | |
| $K_2O$ | 9.56 | 0.949 | 8.90 | 0.886 | 9.79 | 0.968 | 9.77 | 0.967 | | | 9.47 | 0.945 | | | 9.92 | 0.989 | | | 9.53 | 0.959 | 9.53 | 0.959 | | |
| Totals: | 93.49 | 7.813 | 93.34 | 7.799 | 94.56 | 7.968 | 94.45 | 7.883 | | | 94.21 | 7.879 | | | 95.05 | 7.895 | | | 94.58 | 7.922 | 94.58 | 7.922 | | |
| $a_{phlog}$ | 0.0705 | | 0.0561 | | 0.0470 | | 0.0426 | | | | 0.0340 | | | | 0.0354 | | | | 0.0344 | | | | 0.0344 | |
| $a_{ann}$ | 0.0790 | | 0.0803 | | 0.0878 | | 0.0846 | | | | 0.0991 | | | | 0.1233 | | | | 0.1316 | | | | 0.1316 | |
| *Garnets*** | | | | | | | cores | | rims | | cores | | rims | | cores | | rims | | cores | | cores | | rims | |
| $SiO_2$ | | | | | | | 36.94 | 3.012 | 36.57 | 2.972 | 36.18 | 2.961 | 36.97 | 3.008 | 37.27 | 3.015 | 37.95 | 3.052 | 36.54 | 2.947 | 36.54 | 2.947 | 36.52 | 2.926 |
| $Al_2O_3$ | | | | | | | 20.58 | 1.978 | 20.81 | 1.994 | 20.49 | 1.977 | 20.61 | 1.977 | 20.36 | 1.941 | 20.15 | 1.910 | 21.19 | 2.015 | 21.19 | 2.015 | 21.41 | 2.022 |
| FeO | | | | | | | 28.85 | 1.967 | 28.44 | 1.933 | 31.02 | 2.123 | 32.15 | 2.187 | 30.58 | 2.069 | 30.52 | 2.053 | 31.92 | 2.153 | 31.92 | 2.153 | 30.99 | 2.077 |
| $Fe_2O_3$ | | | | | | | 0.00 | 0.00 | 1.01 | 0.062 | 1.66 | 0.102 | 0.13 | 0.008 | 0.49 | 0.030 | 0.00 | 0.00 | 1.50 | 0.091 | 1.50 | 0.091 | 2.08 | 0.125 |
| MgO | | | | | | | 2.31 | 0.281 | 2.53 | 0.306 | 2.73 | 0.333 | 2.36 | 0.286 | 2.26 | 0.272 | 2.26 | 0.271 | 2.39 | 0.287 | 2.39 | 0.287 | 2.37 | 0.283 |
| MnO | | | | | | | 9.51 | 0.657 | 8.92 | 0.614 | 5.78 | 0.401 | 5.54 | 0.382 | 7.93 | 0.543 | 8.71 | 0.593 | 6.18 | 0.422 | 6.18 | 0.422 | 6.59 | 0.447 |
| CaO | | | | | | | 1.18 | 0.103 | 1.36 | 0.118 | 1.19 | 0.104 | 1.75 | 0.153 | 1.50 | 0.130 | 1.32 | 0.114 | 0.98 | 0.085 | 0.98 | 0.085 | 1.39 | 0.119 |
| Totals: | | | | | | | 99.37 | 7.999 | 99.64 | 8.000 | 99.05 | 8.000 | 99.50 | 8.000 | 100.00 | 8.000 | 100.90 | 7.993 | 100.70 | 8.000 | 100.70 | 8.000 | 101.00 | 8.000 |
| $a_{alm}$ | | | | | | | 0.276994 | | 0.255589 | | 0.329122 | | 0.375868 | | 0.309794 | | 0.307476 | | 0.353828 | | 0.353628 | | 0.312903 | |
| $a_{py}$ | | | | | | | 0.000875 | | 0.001124 | | 0.001397 | | 0.000967 | | 0.000790 | | 0.000777 | | 0.000909 | | 0.000909 | | 0.000884 | |
| $a_{gr}$ | | | | | | | 0.000050 | | 0.000076 | | 0.000053 | | 0.000165 | | 0.000097 | | 0.000066 | | 0.000028 | | 0.000028 | | 0.000077 | |

* Biotite-zone samples.

** Calculations of $FeO/Fe_2O_3$; cations and activities were made using the program AX (Holland, personal communication).

Abbreviations in activities: phlog = phlogopite; ann = annite; alm = almandine; py = pyrope; gr = grossular.
Other abbreviations: wt% = wt% of oxide; cat = cations.

Table 3. Electron microprobe analyses of minerals from the staurolite-cordierite-$Al_2SiO_5$ zone, Campus area, Elat Association

| Sample# | 7 | | 7 | | 67 | | 67 | | 70 | | 70 | | 54 | | 54 | | 5 | | 5 | |
|---|---|---|---|---|---|---|---|---|---|---|---|---|---|---|---|---|---|---|---|---|
| | Wt% | Cat. | Wt% | Cat. | Wt% | Cat. | Wt% | Cat. | Wt% | Cat. | Wt% | Cat. | Wt% | Cat. | Wt% | Cat. | Wt% | Cat. | Wt% | Cat. |
| *Biotites* | | | | | | | | | | | | | | | | | | | | |
| $SiO_2$ | 35.05 | 2.664 | | | 35.29 | 2.679 | | | 35.19 | 2.647 | | | 35.18 | 2.633 | | | 34.26 | 2.627 | | |
| $Al_2O_3$ | 20.06 | 1.797 | | | 20.18 | 1.806 | | | 19.90 | 1.765 | | | 21.18 | 1.869 | | | 19.67 | 1.778 | | |
| FeO | 20.27 | 1.288 | | | 19.81 | 1.258 | | | 21.28 | 1.339 | | | 19.21 | 1.203 | | | 21.66 | 1.389 | | |
| $Fe_2O_3$ | 0.00 | 0.00 | | | 0.00 | 0.00 | | | 0.00 | 0.00 | | | 0.00 | 0.00 | | | 0.00 | 0.00 | | |
| MgO | 9.34 | 1.058 | | | 9.65 | 1.092 | | | 9.93 | 1.113 | | | 9.90 | 1.104 | | | 9.01 | 1.030 | | |
| MnO | 0.13 | 0.008 | | | 0.08 | 0.005 | | | 0.10 | 0.006 | | | 0.12 | 0.008 | | | 0.18 | 0.012 | | |
| $TiO_2$ | 1.41 | 0.081 | | | 1.32 | 0.075 | | | 1.35 | 0.078 | | | 1.49 | 0.084 | | | 1.68 | 0.097 | | |
| $Na_2O$ | 0.21 | 0.031 | | | 0.32 | 0.047 | | | 0.19 | 0.028 | | | 0.23 | 0.033 | | | 0.25 | 0.037 | | |
| CaO | 0.02 | 0.002 | | | 0.04 | 0.003 | | | 0.04 | 0.003 | | | 0.06 | 0.005 | | | 0.01 | 0.001 | | |
| $K_2O$ | 9.16 | 0.888 | | | 8.25 | 0.799 | | | 8.97 | 0.861 | | | 8.91 | 0.851 | | | 8.86 | 0.867 | | |
| Totals: | 95.65 | 7.817 | | | 94.94 | 7.765 | | | 96.95 | 7.838 | | | 96.28 | 7.790 | | | 95.58 | 7.838 | | |
| $a_{phlog}$ | 0.0404 | | | | 0.0396 | | | | 0.0447 | | | | 0.0436 | | | | 0.0366 | | | |
| $a_{ann}$ | 0.0730 | | | | 0.0606 | | | | 0.777 | | | | 0.0563 | | | | 0.0898 | | | |
| *Garnets*** | cores | | rims | | cores | | rims | | cores | | rims | | cores | | rims | | cores | | rims | |
| $SiO_2$ | 37.06 | 3.053 | 37.11 | 3.060 | 36.82 | 2.979 | 36.95 | 2.992 | 37.51 | 3.026 | 37.47 | 2.997 | 37.31 | 3.011 | 37.44 | 3.039 | 37.43 | 3.000 | 38.16 | 3.018 |
| $Al_2O_3$ | 19.79 | 1.922 | 19.79 | 1.924 | 21.28 | 2.030 | 21.14 | 2.018 | 20.93 | 1.991 | 21.46 | 2.204 | 20.89 | 1.988 | 20.30 | 1.942 | 21.08 | 1.992 | 21.42 | 1.997 |
| FeO | 31.31 | 2.157 | 31.42 | 2.167 | 33.95 | 2.298 | 34.34 | 2.325 | 30.89 | 2.084 | 32.42 | 2.169 | 31.86 | 2.150 | 32.08 | 2.178 | 32.54 | 2.181 | 32.53 | 2.152 |
| $Fe_2O_3$ | 0.00 | 0.00 | 0.00 | 0.00 | 0.19 | 0.011 | 0.00 | 0.00 | 0.00 | 0.00 | 0.00 | 0.00 | 0.00 | 0.00 | 0.00 | 0.00 | 0.13 | 0.008 | 0.00 | 0.00 |
| MgO | 2.75 | 0.338 | 2.61 | 0.321 | 2.86 | 0.345 | 2.72 | 0.328 | 2.96 | 0.356 | 2.96 | 0.353 | 2.82 | 0.339 | 2.70 | 0.327 | 2.59 | 0.309 | 2.44 | 0.288 |
| MnO | 5.41 | 0.378 | 5.68 | 0.397 | 3.27 | 0.224 | 3.44 | 0.236 | 5.55 | 0.379 | 4.89 | 0.331 | 5.19 | 0.355 | 5.48 | 0.377 | 5.90 | 0.401 | 6.36 | 0.426 |
| CaO | 1.55 | 0.137 | 1.24 | 0.110 | 1.30 | 0.113 | 1.15 | 0.100 | 1.84 | 0.142 | 1.37 | 0.117 | 1.76 | 0.152 | 1.47 | 0.128 | 1.27 | 0.109 | 1.21 | 0.103 |
| Totals: | 97.87 | 7.985 | 97.85 | 7.978 | 99.67 | 8.000 | 99.74 | 7.999 | 99.48 | 7.978 | 100.60 | 7.991 | 99.83 | 7.995 | 89.47 | 7.990 | 100.90 | 8.000 | 102.10 | 7.983 |
| $a_{alm}$ | 0.361750 | | 0.373840 | | 0.446493 | | 0.464702 | | 0.341595 | | 0.382756 | | 0.362043 | | 0.372903 | | 0.376262 | | 0.376521 | |
| $a_{py}$ | 0.001599 | | 0.001358 | | 0.001711 | | 0.001458 | | 0.001974 | | 0.001869 | | 0.001667 | | 0.001437 | | 0.001202 | | 0.000999 | |
| $a_{gr}$ | 0.000131 | | 0.000067 | | 0.000077 | | 0.000053 | | 0.000156 | | 0.000089 | | 0.000183 | | 0.000106 | | 0.000065 | | 0.000055 | |
| *Plagioclases* | | | | | | | | | | | | | | | | | | | | |
| $SiO_2$ | 64.42 | 2.804 | | | 63.41 | 2.795 | | | 60.56 | 2.694 | | | 60.59 | 2.681 | | | 64.46 | 2.798 | | |
| $Al_2O_3$ | 23.02 | 1.181 | | | 22.98 | 1.194 | | | 24.78 | 1.299 | | | 25.22 | 1.316 | | | 23.45 | 1.200 | | |
| $Na_2O$ | 8.89 | 0.750 | | | 8.19 | 0.700 | | | 7.99 | 0.689 | | | 7.95 | 0.682 | | | 8.52 | 0.717 | | |
| CaO | 5.18 | 0.242 | | | 5.68 | 0.268 | | | 6.63 | 0.316 | | | 6.75 | 0.320 | | | 5.24 | 0.244 | | |
| $K_2O$ | 0.09 | 0.005 | | | 0.00 | 0.00 | | | 0.09 | 0.005 | | | 0.08 | 0.005 | | | 0.11 | 0.006 | | |
| Totals: | 101.60 | 4.983 | | | 100.20 | 4.958 | | | 100.00 | 5.004 | | | 100.60 | 5.004 | | | 101.80 | 4.964 | | |
| | | | | | | | | | | | | | | | | | 0.69 | | | |
| $a_{albite}$ | 0.70 | | | | 0.67 | | | | 0.62 | | | | 0.62 | | | | 0.42 | | | |
| $a_{anorth}$ | 0.40 | | | | 0.47 | | | | 0.54 | | | | 0.55 | | | | | | | |

| Sample# | 49 | | 49 | | 16 | | 16 | | 30 | | 30 | | 40 | | | | Staurolites 7 | | Staurolites 67 | | Cordierite 67 | |
|---|---|---|---|---|---|---|---|---|---|---|---|---|---|---|---|---|---|---|---|---|---|---|
| | Wt% | Cat. | Wt% | Cat. | Wt% | Cat. | Wt% | Cat. | Wt% | Cat. | Wt% | Cat. | Wt% | Cat. | | | Wt% | Cat. | Wt% | Cat. | Wt% | Cat. |
| *Biotites* | | | | | | | | | | | | | | | | | | | | | | |
| $SiO_2$ | 35.12 | 2.654 | | | 34.74 | 2.646 | | | 35.62 | 2.742 | | | 35.11 | 2.680 | | | 27.49 | 4.019 | 27.17 | 4.021 | 47.52 | 6.868 |
| $Al_2O_3$ | 20.95 | 1.867 | | | 20.00 | 1.796 | | | 18.74 | 1.701 | | | 19.70 | 1.773 | | | 53.58 | 9.251 | 50.69 | 9.080 | 31.82 | 5.416 |
| FeO | 18.84 | 1.191 | | | 19.83 | 1.263 | | | 18.92 | 1.218 | | | 19.16 | 1.224 | | | 13.18 | 1.613 | 13.93 | 1.766 | 8.69 | 1.076 |
| $Fe_2O_3$ | 0.00 | 0.00 | | | 0.00 | 0.00 | | | 0.00 | 0.00 | | | 0.00 | 0.00 | | | 0.00 | 0.00 | 0.00 | 0.00 | 0.00 | 0.00 |
| MgO | 9.74 | 1.097 | | | 9.89 | 1.123 | | | 10.05 | 1.153 | | | 0.04 | 1.142 | | | 1.74 | 0.379 | 1.75 | 0.396 | 8.26 | 0.890 |
| MnO | 0.08 | 0.005 | | | 0.14 | 0.009 | | | 0.12 | 0.008 | | | 0.11 | 0.007 | | | 0.21 | 0.026 | 0.12 | 0.016 | 0.21 | 0.026 |
| $TiO_2$ | 1.30 | 0.074 | | | 1.52 | 0.087 | | | 1.30 | 0.075 | | | 1.40 | 0.080 | | | 0.66* | 0.071 | 0.44* | 0.049 | 0.00 | 0.00 |
| $Na_2O$ | 0.13 | 0.019 | | | 0.25 | 0.037 | | | 0.17 | 0.025 | | | 0.12 | 0.018 | | | | | | | 0.44 | 0.062 |
| CaO | 0.07 | 0.006 | | | 0.03 | 0.002 | | | 0.20 | 0.016 | | | 0.03 | 0.002 | | | | | | | 0.03 | 0.005 |
| $K_2O$ | 9.02 | 0.870 | | | 8.70 | 0.846 | | | 8.29 | 0.814 | | | 8.97 | 0.873 | | | | | | | 0.00 | 0.00 |
| Totals: | 95.25 | 7.783 | | | 95.10 | 7.810 | | | 93.41 | 7.752 | | | 94.66 | 7.799 | | | 96.86 | 15.36 | 94.10 | 15.31 | 96.97 | 15.23 |
| $a_{phlog}$ | 0.0434 | | | | 0.0459 | | | | 0.0489 | | | | 0.0501 | | | | | | | | | |
| $a_{ann}$ | 0.0555 | | | | 0.0654 | | | | 0.0576 | | | | 0.0617 | | | | | | | | | |
| *Garnets*** | cores | | rims | | cores | | rims | | cores | | rims | | cores | | rims | | Staurolites 70 | | Staurolites 49 | | Staurolites 40 | |
| $SiO_2$ | 37.05 | 3.034 | 37.20 | 3.020 | 38.28 | 3.055 | 37.82 | 3.005 | 37.28 | 3.001 | 36.00 | 2.922 | 36.97 | 3.017 | 36.94 | 3.008 | 2.47 | 4.032 | 27.18 | 4.025 | 27.02 | 3.981 |
| $Al_2O_3$ | 20.01 | 1.932 | 20.53 | 1.965 | 20.72 | 1.949 | 21.70 | 2.033 | 20.85 | 1.979 | 20.80 | 1.990 | 20.11 | 1.935 | 20.43 | 1.961 | 52.77 | 9.120 | 52.63 | 9.186 | 53.54 | 9.293 |
| FeO | 31.39 | 2.150 | 32.31 | 2.194 | 31.73 | 2.118 | 31.72 | 2.108 | 32.38 | 2.179 | 31.13 | 2.113 | 31.563 | 2.152 | 32.39 | 2.206 | 13.60 | 1.668 | 13.40 | 1.659 | 13.08 | 1.611 |
| $Fe_2O_3$ | 0.02 | 0.011 | 0.00 | 0.00 | 0.00 | 0.00 | 0.00 | 0.00 | 0.33 | 0.020 | 2.71 | 0.165 | 0.51 | 0.031 | 0.39 | 0.024 | 0.00 | 0.00 | 0.00 | 0.00 | 0.00 | 0.00 |
| MgO | 3.00 | 0.366 | 2.59 | 0.357 | 2.93 | 0.348 | 2.80 | 0.332 | 3.06 | 0.357 | 2.84 | 0.344 | 3.10 | 0.377 | 2.96 | 0.359 | 2.35 | 0.524 | 1.95 | 0.431 | 1.92 | 0.421 |
| MnO | 5.58 | 0.387 | 4.94 | 0.340 | 5.35 | 0.362 | 5.64 | 0.380 | 4.98 | 0.340 | 5.28 | 0.363 | 5.16 | 0.357 | 4.80 | 0.331 | 0.18 | 0.022 | 0.19 | 0.024 | 0.19 | 0.024 |
| CaO | 1.49 | 0.131 | 1.41 | 0.123 | 1.63 | 0.139 | 1.43 | 0.122 | 1.33 | 0.115 | 1.18 | 0.103 | 1.50 | 0.131 | 1.28 | 0.112 | 0.44* | 0.048 | 0.51* | 0.056 | 0.39* | 0.042 |
| Totals: | 98.54 | 8.000 | 99.34 | 7.998 | 100.60 | 7.971 | 101.10 | 7.797 | 100.20 | 8.000 | 99.93 | 8.000 | 98.88 | 8.000 | 99.19 | 8.000 | 94.10 | 15.41 | 95.86 | 15.38 | 96.14 | 15.35 |
| $a_{alm}$ | 0.349252 | | 0.379490 | | 0.356443 | | 0.362155 | | 0.369321 | | 0.317573 | | 0.344790 | | 0.379067 | | | | | | | |
| $a_{py}$ | 0.001960 | | 0.001855 | | 0.001840 | | 0.001603 | | 0.001992 | | 0.001524 | | 0.002126 | | 0.001842 | | | | | | | |
| $a_{gr}$ | 0.000112 | | 0.000096 | | 0.000147 | | 0.000099 | | 0.000079 | | 0.000053 | | 0.000116 | | 0.000072 | | | | | | | |
| *Plagioclases*** | | | | | | | | | | | | | | | | | | | | | | |
| $SiO_2$ | 60.50 | 2.685 | | | 62.68 | 2.720 | | | 62.02 | 2.763 | | | 61.03 | 2.684 | | | | | | | | |
| $Al_2O_3$ | 24.99 | 1.307 | | | 25.10 | 1.284 | | | 23.01 | 1.209 | | | 25.27 | 1.310 | | | | | | | | |
| $Na_2O$ | 8.21 | 0.706 | | | 8.37 | 0.704 | | | 8.72 | 0.753 | | | 8.42 | 0.718 | | | | | | | | |
| CaO | 6.59 | 0.313 | | | 6.02 | 0.280 | | | 5.89 | 0.281 | | | 6.49 | 0.306 | | | | | | | | |
| $K_2O$ | 0.08 | 0.005 | | | 0.10 | 0.006 | | | 0.08 | 0.005 | | | 0.07 | 0.004 | | | | | | | | |
| Totals: | 100.40 | 5.017 | | | 102.20 | 4.993 | | | 99.72 | 5.011 | | | 101.30 | 5.022 | | | | | | | | |
| $a_{albite}$ | 0.63 | | | | 0.65 | | | | 0.67 | | | | 0.64 | | | | | | | | | |
| $a_{anorth}$ | 0.53 | | | | 0.48 | | | | 0.46 | | | | 0.51 | | | | | | | | | |

* Analyses (staurolites only) are for zinc as ZnO. ** Calculations of FeO and $Fe_2O_3$, cations, and activities were made using the program AX (Holland, personal communication).
Abbreviations in activities: phlog = phlogopite; ann = annite; alm = almandine; py = pyrope; gr = grossular; anorth = anorthite. Other abbreviations: wt% = wt % of oxide; cat = cations.

Analyses are reported as oxides (wt%) and cations (cat). Allocation of $Fe^{3+}$ for garnets is made assuming 8 cations, and for biotites, assuming 7 cations (except for $Na^+$, $K^+$, and $Ca^{2+}$).

Since the fractionation of Mg and Fe between garnet and biotite governs the thermometric estimates and Ca partition between garnet and plagioclase governs the pressure (barometric) estimates, the petrographic relations among these minerals are of prime importance. Biotite-plagioclase occurs in all pelitic rock types, whereas garnet occurs in micaceous varieties of garnet-zone rocks and in most staurolite-cordierite-$Al_2SiO_5$-zone rocks. Biotite and plagioclase define the S1 cleavage in all three zones, and consequently their growth must at least have commenced during the first folding phase. Shimron (1972) identified a continuous history of biotite-plagioclase and garnet growth that commenced with this phase and continued beyond the second phase. This raises the question of what stage of the metamorphic history will be represented in the chemical analyses of these minerals. It is a general assumption in metamorphic petrology that the facies assemblages developed in a rock represent maximum entropy conditions, which are usually close to maximum $T$ conditions attained by that rock. In the absence of strong evidence for retrogradation or a metamorphic overprint, it may be presumed that the chemical fractionations among minerals are close to equilibrium at maximum $P$–$T$ conditions. The interpretation of the meaning of the element fractionation relationships, however, can be derived only from a detailed analysis of chemical profiles in minerals and their relationship to the history of metamorphism in the area. Some attempts to constrain the meaning of the $P$–$T$ data deduced in this study will be presented in the ensuing sections.

Staurolite, cordierite, andalusite, and sillimanite occur in the highest grades of metamorphism. There is no evidence for the development of very high grade cordierite-biotite-K-feldspar parageneses.

## RESULTS AND DISCUSSION

### Mineral chemistry

The chemical compositions of minerals given in Tables 2 and 3 are typical of those of pelitic rocks, almandine-rich garnet, Fe-rich staurolite, plagioclase ~$An_{30}$, and biotite with Mg/(Fe+Mg) ~0.4–0.5. The mineral chemistries of garnets, biotites, staurolites, and one cordierite are plotted in Figs. 3 and 4 on AFM projections, together with tie lines joining coexisting

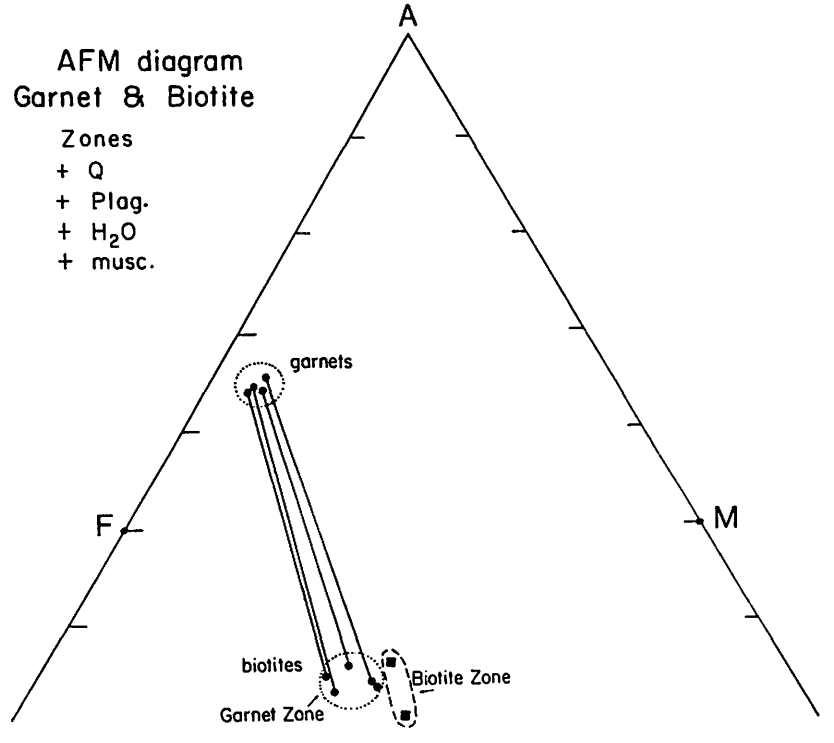


Fig. 3. AFM projection from muscovite showing compositions of biotites and garnets from the garnet and biotite zone samples. Tie lines joining coexisting minerals are shown in the diagram.

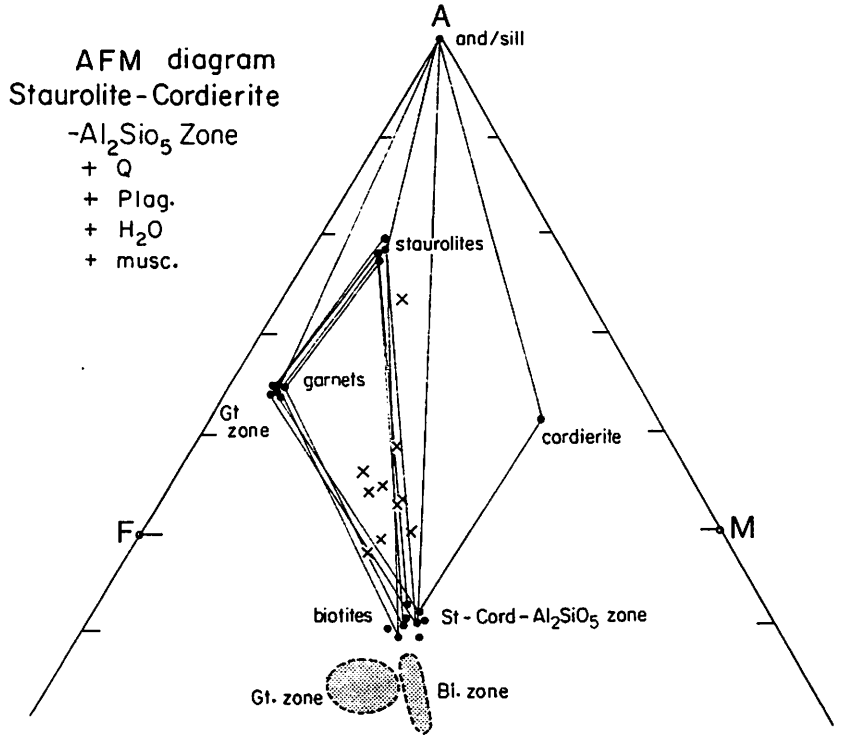


Fig. 4. AFM projection from muscovite showing compositions of biotites, garnets, staurolites, and a cordierite from the staurolite-cordierite-$Al_2SiO_5$ zone in the SW of the Campus area. Representative tie lines joining coexisting assemblages are shown in the diagram. Whole-rock analyses of staurolite-cordierite-bearing rocks (indicated by an x) are taken from Shimron (1972) after allowance for the $Al_2O_3$ in plagioclase in addition to that in muscovite. Shaded areas show biotite compositions from the biotite and garnet zones.

phases. The analyses of the garnet are rim compositions (Tables 2 and 3).

Garnet-biotite pairs from the garnet-zone samples show a regular distribution of tie lines (Fig. 3) indicating that exchange chemistry shows no irregularities. The highest Mg/(Fe+Mg) values are for the garnet-biotite of sample #88 located just south of the "garnet In" line. The garnet-zone biotites are noticeably more Fe-rich than the 2 biotite samples analyzed from the biotite zone.

Garnet, biotite, staurolite, and cordierite analyses from the staurolite-cordierite-$Al_2SiO_5$-zone samples are shown in Fig. 4. Again, within the limits of analytical error, a regular distribution of tie lines is observed, suggesting that all analyzed parageneses are in equilibrium. Biotites have Mg/(Mg+Fe) ratios similar to those of the biotite zone, i.e., are richer in Mg than the biotites of the garnet zone. Garnet-rim compositions of samples from the garnet zone and the staurolite-cordierite-$Al_2SiO_5$ zone are similar (Fig. 4).

Sample #67 is a four-phase staurolite-cordierite-garnet-biotite assemblage in the AFM diagram. Although, strictly, four-phase equilibrium assemblages should not exist on an AFM projection, the assemblage is commonly observed in medium-to-high-grade pelitic metamorphic rocks. Bulk-rock chemical analyses of staurolite-cordierite-$Al_2SiO_5$ grade rocks given by Shimron (1972) are plotted on the AFM diagram of Fig. 4. The analyses fall either within the staurolite–biotite–garnet triangle or near the staurolite–biotite tie lines. As a whole, the bulk compositional data favor the formation of staurolite–biotite–garnet parageneses, with cordierite growth being more sporadic and possibly related to local variations in rock chemistry.

As noted, garnets show significant chemical compositional differences between cores and rims. The zonation patterns with respect to $MgFe^{-1}$ and Ca exchange are shown in Fig. 5. Staurolite-cordierite-$Al_2SiO_5$-zone samples show consistent relationships between cores and rims, with cores being characterized by higher $MgFe^{-1}$ and *X*. Ca than rims. In the garnet-zone samples relationships are more varied, although in each case three out of four samples show lower $MgFe^{-1}$ and *X*. Ca in rims.

These near-systematic variations of $MgFe^{-1}$ and *X*. Ca are an expression of the buffering of these com-

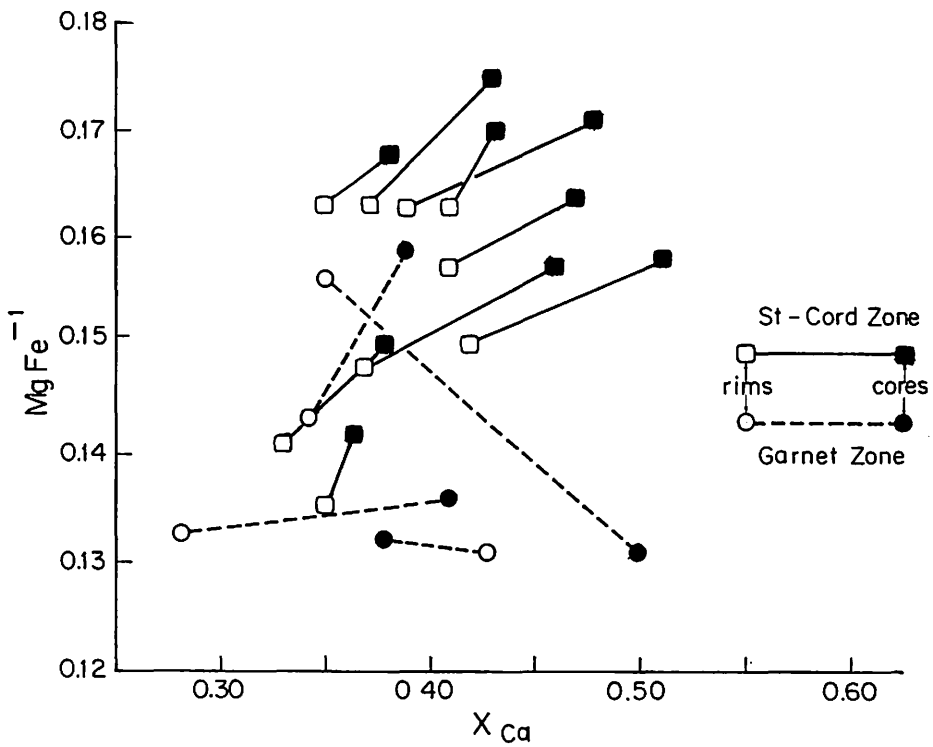


Fig. 5. A plot of $MgFe^{-1}$ against *X*. Ca ( = Ca/(Ca+Mg+Fe+Mn)) in the cores and rims of garnets. Data sources: Tables 2 and 3.

positional variables by reactions such as:

$$\underset{\text{almandine}}{Fe_3Al_2Si_3O_{12}{}^{gt}} + \underset{\text{phlogopite}}{KMg_3AlSi_3O_{10}(OH)_2{}^{bi}} \rightleftharpoons \underset{\text{pyrope}}{Mg_3Al_2Si_3O_{12}{}^{gt}} + \underset{\text{annite}}{KFe_3AlSi_3O_{10}(OH)_2{}^{bi}} \quad (1)$$

$$\underset{\text{grossular}}{Ca_3Al_2Si_3O_{12}{}^{gt}} + \underset{\text{andalusite/sillimanite}}{2Al_2SiO_5} + SiO_2 \rightleftharpoons \underset{\text{anorthite}}{3CaAl_2Si_2O_6{}^{plag}} \quad (2)$$

Since the modal proportions of biotite and plagioclase in the pelitic rocks are usually significantly greater than those of garnet and other phases bearing Mg, Fe, or Ca, the biotite and plagioclase act as the compositional buffers for $MgFe^{-1}$ and Ca exchange, respectively. Consequently, during continuous exchange processes, the composition of garnets will change, but those of biotites and plagioclases will remain relatively constant. Mg, Fe, and Ca compositional relationships between chemically homogeneous biotites and plagioclases and garnet cores and rims can be considered to express a segment of the continuous exchange history, i.e., *P–T* path, of the metamorphism.

The AFM compositions of biotites and garnets from the Elat Association are compared with those of the garnet and staurolite-$Al_2SiO_5$ (andalusite) zones of the Wadi Kid complex, SE Sinai, in Fig. 6. The garnets from Wadi Kid grade into more Mg-rich compositions during the transition from garnet zone into staurolite-$Al_2SiO_5$ conditions and similarly the biotites show evidence of a slight enrichment in Mg. This would be consistent with the transformation from garnet zone to staurolite-bearing assemblages by continuous prograde reactions such as: chlorite + muscovite $\rightleftharpoons$ staurolite + biotite + quartz + water, whereby disappearance of chlorite and formation of staurolite with increase in temperature leads to a progressive enrichment of Mg in the garnet. In contrast, the Elat minerals do not show clear evidence of such a transition: garnet analyses from garnet and staurolite-cordierite-$Al_2SiO_5$ zones overlap in chemical composition and biotites have distinctly different compositions. Thus, unlike the Wadi Kid samples, it does not appear possible to relate the garnet and staurolite-cordierite-$Al_2SiO_5$ zones of the Elat Association by any simple continu-

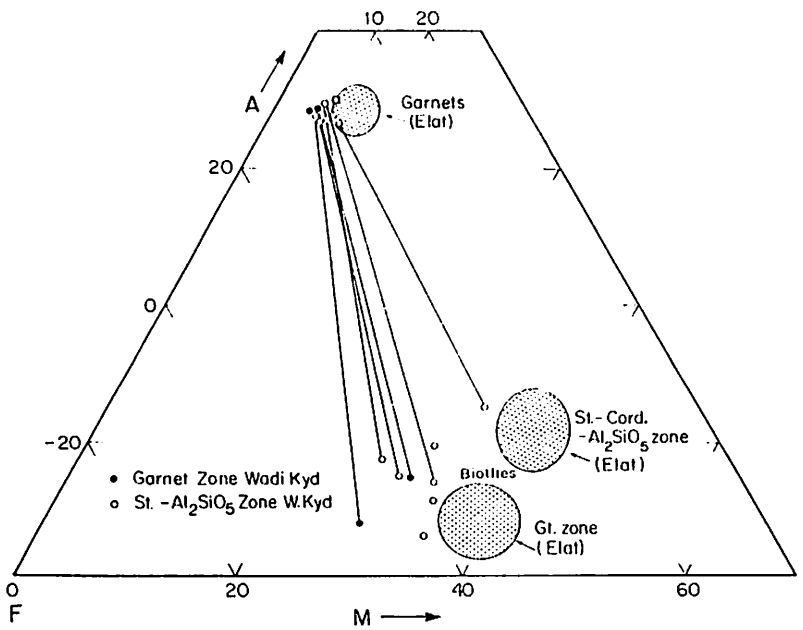


Fig. 6. Garnet-biotite portion of the AFM triangle showing the compositions of garnets and biotites from the garnet and staurolite-$Al_2SiO_5$ zones of central Wadi Kid, SE Sinai. Data source: Reymer et al. (1984b). Comparative fields for Elat Association minerals (Figs. 3 and 4) are shown as shaded areas in the diagram.

ous reaction relationship. Either the bulk compositions of the rocks of the two zones are different or a metamorphic break separates them.

### Geothermobarometry

The determination of temperatures is based on the garnet–biotite $MgFe^{-1}$ exchange reaction (equation 1) and barometry on the partitioning of Ca between garnet and plagioclase (equation 2). The geothermobarometric relations are expressed by the standard thermodynamic equation: $\Delta H^0 - T\Delta S^0 + P\Delta V^0 + RT \ln K = 0$. Thermodynamic properties for the garnet–biotite exchange reaction are from Ferry and Spear (1978): $\Delta H^0 = -52.108$ kJ; $\Delta S^0 = -19.51$ J/K; $\Delta V^0 = -0.057$ J/bar. Thermodynamic relations for the garnet–plagioclase reaction with sillimanite as the $Al_2SiO_5$ phase are from the thermodynamic data set of Holland and Powell(1985) and Powell and Holland (1988): $\Delta H^0 = 20.570$ kJ; $\Delta S^0 = 109.8$ J/K; $\Delta V^0 = 5.466$ J/bar.

The choice of sillimanite in the pressure calculations requires some detailed comment. Both andalusite and sillimanite occur in the staurolite-cordierite-$Al_2SiO_5$ zone. Andalusite porphyroblasts form as prograde minerals, whereas in the rocks we examined sillimanite in its fibrolite form is most frequently observed as apparent overgrowths of biotite. These observations are consistent with those of Shimron (1972) who also noted the tendency for sillimanite to occur as overgrowths with late (retrograde) muscovite. Textural association of biotite with sillimanite is commonly observed in high-grade schists of the Dalradian of Scotland (Mason, 1978). Most interpretations of this texture have favored sillimanite as post-dating the biotite; Carmichael (1969), however, has proposed a complex ion-exchange mechanism whereby simultaneous sillimanite and biotite growth occur during the transformation from kyanite to sillimanite-stable conditions.

Thus, it is not clear whether the andalusite-sillimanite presence in the Elat schists represents a genuine prograde transformation with sillimanite indicating peak metamorphic conditions, or whether sillimanite growth occurred late, perhaps as late as the time of intrusion of the Elat granite (Garfunkel, 1980). Despite these uncertainties the calculations were made using sillimanite simply because the results show that peak metamorphic conditions are largely within the sillimanite field. The calculations could have been made using andalusite thermodynamic data, but the results would have been within 0.1 to 0.2 kbar of those determined using sillimanite data, and still within the sillimanite field. If it is unequivocally shown in the future that all sillimanite growth is late and not associated with peak metamorphic conditions, then the results presented in this study will clearly imply that andalusite was metastably preserved at the

highest grades of metamorphism.

Some of the analyzed samples from the staurolite-cordierite-$Al_2SiO_5$ zone do not include sillimanite (Table 1). However, sillimanite and andalusite are sufficiently ubiquitous phases in the zone that it is a reasonable assumption that the activity of $Al_2SiO_5$ ($a_{Al_2SiO_5}$) =1. Since $Al_2SiO_5$ polymorphs have not been observed in the garnet zone, the assumption that $a_{Al_2SiO_5} = 1$ is not justifiable and no pressure calculations are made for the samples from this zone.

Equilibrium constants, $K$, for the exchange reactions are calculated using the following activity models: biotite — ideal mixing on sites; garnet — regular solution model of Newton and Haselton (1981); plagioclase — solution model of Newton and Haselton (1981). The activities were calculated using the program AX (Holland, personal communication) and are given in Tables 2 and 3.

The iterated pressure–temperature calculations using both garnet core and rim activities are given in Table 4. In error propagation calculations, individual temperature determinations are assumed to carry a maximum error of ±50°C and corresponding errors in single pressures are about ±1.1 kbar.

Mean $P$ and $T$ values are given for the staurolite-cordierite-$Al_2SiO_5$-zone samples together with propagated errors.

*Pressures and temperatures in the staurolite-cordierite-$Al_2SiO_5$ zone.* The garnet rim-biotite temperatures range from 554 to 621°C and average 583 ± 25°C (propagated errors). The distribution of temperatures is shown in Fig. 7. No obvious spatial trend of temperatures is observed, either from the point of view of higher temperatures near the contact with the granite gneiss or, alternatively, towards the center of the unit.

Rim pressures average 3.84 ± 0.69 kbar, corresponding to a depth of burial of ~14 km at an assumed rock density of 2.75. Temperatures and pressures deduced from garnet cores are systematically higher than those from rims, averaging 604 ± 26°C and 4.60 ± 0.8 kbar. The core–rim fractionations in garnet porphyroblasts thus identify a segment of the metamorphic history which involves a slight reduction in $P$–$T$ conditions.

The $P$–$T$ conditions deduced for the Elat samples are plotted in Fig. 8, together with the $Al_2SiO_5$ diagram and limiting conditions for the breakdown of muscovite and quartz to K-feldspar + sillimanite. Arrows represent a schematic segment of the $P$–$T$ path of the rocks, assuming that kyanite was never present and that garnet core conditions represent the peak of metamorphism. The $P$–$T$ conditions are within the sillimanite field for garnet cores and around the andalusite/sillimanite boundary for garnet rims. Muscovite breakdown conditions were never attained.

It is assumed here (see Fig. 8) that temperatures and pressures given by garnet cores represent peak thermal conditions in this zone. Assigning a condition to the slightly lower temperatures and pressures given by garnet rims presents a problem. The temperatures are too high to represent the later upper greenschist facies overprint. It is possible that they represent a tectonic uplifting of the staurolite-cordierite-$Al_2SiO_5$ zone onto the granite gneiss. This would result in a pressure decrease and, since temperature effects of contact metamorphism are not observed with the granite gneiss, would have brought the staurolite-cordierite-$Al_2SiO_5$-zone rocks in contact with granites that had already undergone cooling from intrusion temperatures. However, it is also possible that the slightly lower $P$–$T$ conditions given by the rims simply represent a stage of cessation of exchange during the cooling and uplift of the complex.

To explore the relevance of the results, it is instructive to compare the temperatures and pressures deduced for the Elat area with those obtained for the staurolite-$Al_2SiO_5$ zone of Wadi Kid (Fig. 1). To make a

Table 4. $P$–$T$ estimates for the Elat metamorphic complex

| Sample # | $T$ °C[1] rims$^{gt}$ | $P$ kbar[2] rims$^{gt}$ | $T$ °C[1] cores$^{gt}$ | $P$ kbar[2] cores$^{gt}$ |
|---|---|---|---|---|
| *Garnet Zone* | | | | |
| 88[3] | 586 | | 629 | |
| 94[3] | 673 | | 610 | |
| 272[3] | 628 | | 630 | |
| 93[3] | 642 | | 658 | |
| *Staurolite-cordierite-$Al_2SiO_5$ zone* | | | | |
| 7 | 595 | 4.70 | 615 | 5.84 |
| 70 | 621 | 4.08 | 646 | 5.11 |
| 67 | 554 | 2.84 | 575 | 3.50 |
| 54 | 560 | 3.71 | 580 | 4.60 |
| 5 | 592 | 4.18 | 615 | 4.65 |
| 49 | 586 | 3.95 | 604 | 4.34 |
| 16 | 585 | 4.44 | 604 | 5.10 |
| 30 | 572 | 2.98 | 587 | 3.63 |
| 40 | 580 | 3.68 | 612 | 4.62 |
| Mean[4] | 583 ± 25 | 3.84 ± 0.69 | 604 ± 26 | 4.60 ± 0.80 |

[1] Individual $T$ estimates are assumed to carry a maximum uncertainty of ±50°C.

[2] Individual $P$ estimates have an uncertainty of ±1.1 to 1.2 kbar.

[3] $T$ calculated for assumed $P$ of 3.8 kbar (rims) and 4.6 kbar (cores).

[4] Includes propagated errors.

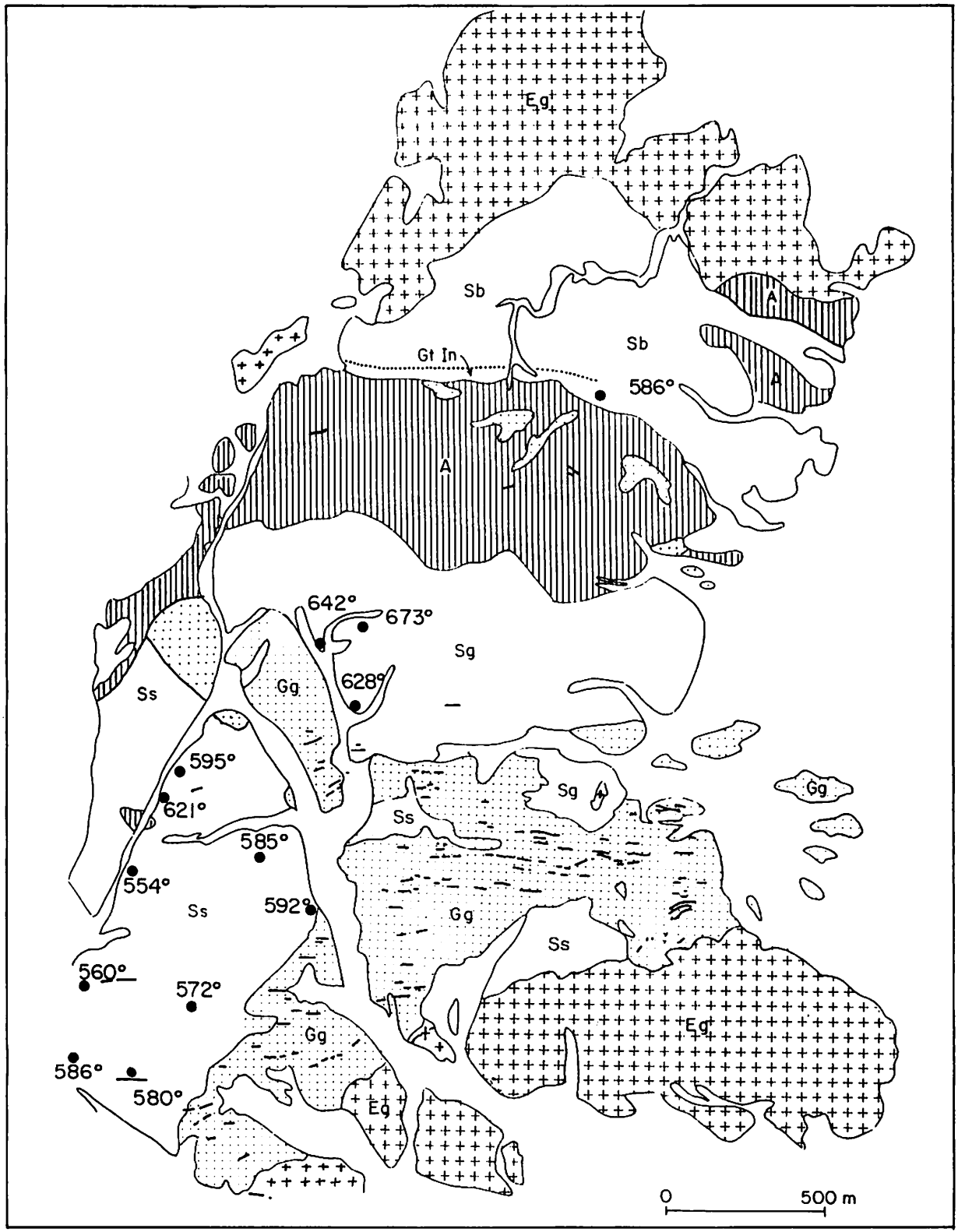


Fig. 7. Distribution of measured garnet (rim)-biotite temperatures in the study area. Garnet core temperatures follow an approximately similar distribution, but with temperatures ~20°C higher. Legend: see Fig. 1.

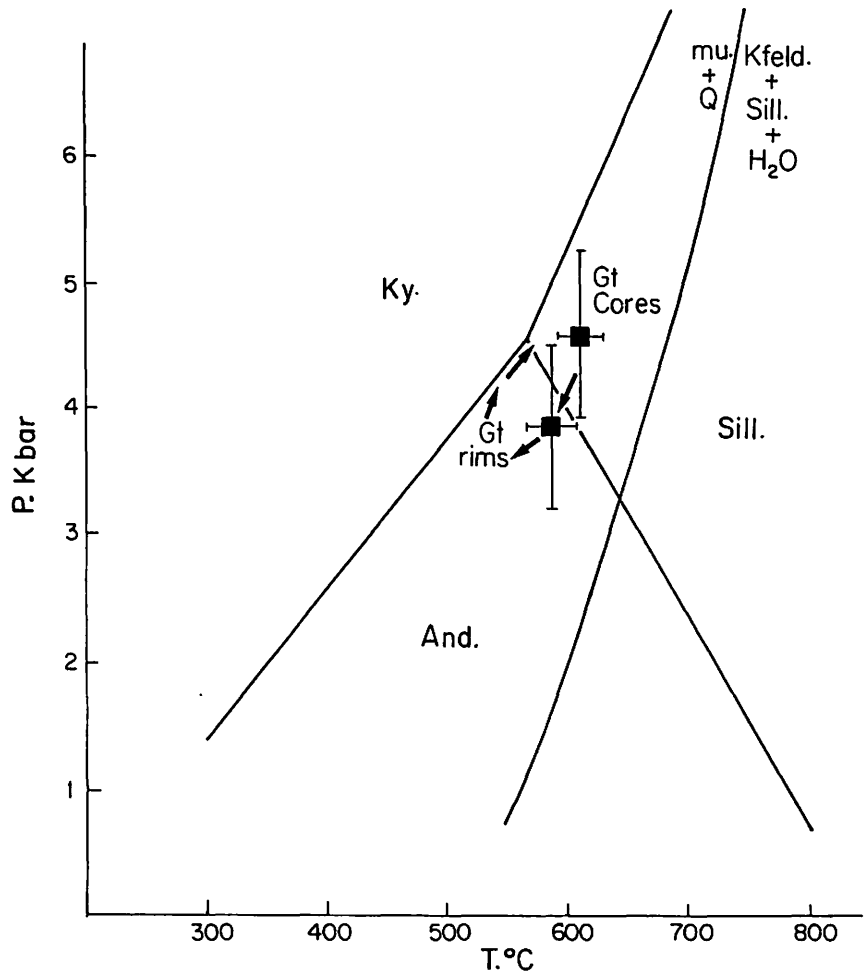


Fig. 8. *P–T* diagram showing mean conditions deduced for staurolite-cordierite-$Al_2SiO_5$ zone samples, using garnet core and garnet rim analyses (Table 4). The $Al_2SiO_5$ diagram and curve for the reaction of muscovite + quartz $\rightleftharpoons$ K-feldspar + sillimanite + water are calculated from the thermodynamic data sets and procedures of Holland and Powell (1985) and Powell and Holland (1988).

valid comparison it was first necessary to recalculate the *P–T* values for Wadi Kid from the original data of Reymer et al. (1984b), using the more accurate models for garnet activities of this study and the more well-constrained thermodynamic data of the Powell and Holland (1988) data set. The mean conditions deduced for Wadi Kid are given in Table 5. Rim temperatures average 580 ± 36°C (compared to 563°C deduced by Reymer et al., 1984b) and are quite similar to those for the Elat schists. Unlike the Elat schists, however, no regular pattern of chemical zonation is found in garnets. Thus, although core analyses give an average temperature of 568°C, slightly lower than that given by rims, a priori they do not give any clear indication of their relevance. The evidence presented earlier of progressive prograde development of garnet into staurolite-zone conditions in Wadi Kid (Fig. 6) is, however, consistent with the core analysis giving slightly lower temperatures than rims.

Pressures deduced from garnet rims from Wadi Kid staurolite-zone samples average 4.5 ± 0.8 kbar. They are higher than the estimate of 3.2 kbar made by Reymer et al. (1984b) mainly because of different models of garnet and plagioclase activities used in this calculation and partly because Reymer et al. (1984b) made no allocation of $Fe^{2+}/Fe^{3+}$, assuming all Fe to be divalent. The pressures deduced for Wadi Kid garnet cores are the same as for garnet rims, and show no evidence of the retrograde higher-to-lower-pressure transition evident in Elat samples.

As a whole, conditions deduced for Wadi Kid and Elat staurolite-bearing samples are almost the same. Garnet core analyses in the Elat samples point to slightly higher peak metamorphic temperatures.

Table 5. Comparative $P$–$T$ estimates for the garnet and staurolite-$Al_2SiO_5$ zones of central Wadi Kid*

| | Garnet zone | Staurolite-$Al_2SiO_5$ zone |
|---|---|---|
| $T^+$ (cores) | 530 ± 52°C | 568 ± 41°C |
| $T^+$ (rims) | 533 ± 41°C | 580 ± 36°C |
| $P^+$ (cores) | | 4.55 ± 0.9 kbar |
| $P^+$ (rims) | | 4.52 ± 0.8 kbar |

* Recalculated from original EPMA data presented in Reymer et al. (1984b), using activity–compositional models used in present study.

\+ Calculations made with analyses of garnet rims and cores, respectively.

An additional comparison that can be made is with temperatures deduced for high-grade metamorphism in the Wadi Magrish area, NE Sinai, ~25 km south of the study area. The Wadi Magrish area includes migmatites, gneisses, and schists which form part of a belt of igneous and metamorphic rocks stretching south from Elat (Fig. 1a), between Wadi Twaiba and Wadi Um Mara (Eyal, 1976, 1980). Similarities between lithologies, structures, and metamorphism in this belt with those of the Elat Association lead Garfunkel (1970) and Eyal (1976, 1980) to consider that they represent the same metamorphic terrain which was disrupted by Late Cenozoic faulting. The geochemistry and mineralogy of the Wadi Magrish migmatite-gneiss-schist association was studied by Amit (1975). The pelitic schists are andalusite-staurolite-garnet-biotite bearing, i.e., similar in grade to those studied here; the migmatites were considered to be the result of metamorphic differentiation of schists (Amit, 1975). Mg $Fe^{-1}$ fractionations between garnet and biotite (Amit, 1975; Amit and Eyal, 1976) can be used to calculate temperatures (as above) although, unlike the Elat and Wadi Kid schists, occasional samples give anomalously high temperatures (e.g., >850°C in migmatites and gneisses). After selecting out apparently disequilibrium results, the following assessments of temperatures can be made: schists — 580 ± 35°C; (Fiord) gneisses — 670 ± 30°C; migmatites — 760 ± 35°C. The temperatures of schist equilibration compare well with those deduced for similar-grade rocks in Elat and Wadi Kid. The temperatures deduced for migmatites are within the range proposed for the onset of dehydration-melting of biotite schists in andalusite-sillimanite-series rocks (Thompson, 1982) and, although they are consistent with the proposal of Amit (1975) that metamorphic differentiation played a major role in their formation, they do not fully rule out the occurrence of slight degrees of melting.

*Garnet zone temperatures.* Temperatures given by garnet-zone samples (garnet rims) range from 586°C for the one sample (#88) north of the pelite/amphibolite contact to 630–670°C for the three other samples located near the contact with the granite gneiss (Table 4, Fig. 6). Garnet core temperatures lack any systematic relationship to rim temperatures.

Temperatures in the range 630–670°C are not only higher than found in staurolite-cordierite-$Al_2SiO_5$-zone samples, but are also significantly higher than generally accepted for garnet-zone conditions. At first glance, therefore, it would appear that temperatures are anomolous, i.e., the $MgFe^{-1}$ fractionations are disequilibrium. However, there are a number of arguments which favor their acceptance. First, the distribution of garnet–biotite lines on the AFM diagram is uniform and consistent with exchange equilibrium. Second, the relationship between garnet-zone rocks and the granite gneiss is intrusive and the contact is marked in several places by the appearance of migmatite textures, possibly indicative of high temperatures.

By way of contrast to the Elat area garnet zone samples, garnet grade samples from the Wadi Kid area give a mean temperature of 533 ± 41°C (Table 5). Additionally, it was shown that the chemical compositions of the Wadi Kid mineral phases are consistent with a continuous reaction relationship between garnet and staurolite-$Al_2SiO_5$ zones (Fig. 6). In Elat, we do not observe evidence of such a relationship, neither from the point of view of chemistry (Fig. 6), nor from the point of view of field relations, since in the Elat area the garnet and staurolite-cordierite-$Al_2SiO_5$ zones are never found in mutual contact.

The alternative interpretation of the garnet-zone temperatures is that they represent the thermal effects of the intrusion of the granite gneiss. It is notable that the slightly lower temperature of 580°C is obtained from the one sample not located in the vicinity of an exposed contact. Even so, this temperature is somewhat higher than normally observed for garnet-zone conditions and may reflect some heat input from the granite. It can be noted that several outcrops of granite intruded into the amphibolite are exposed (Fig. 1c).

The problem with this interpretation remains the quartz-plagioclase-biotite-muscovite ± garnet mineralogy of the garnet-zone samples. The absence of staurolite does not present a problem since temperatures of ≥620°C would normally be above the stability conditions for the mineral. However, both cordierite and sillimanite might be anticipated, but in fact, apart from one fibrolitic sillimanite occurrence reported by Shimron (1972), there is no evidence for their presence. It

may be that a combination of factors are involved in inhibition of an obvious high-temperature mineralogy. The granite gneiss body is restricted in size and its thermal recrystallization effects on the metasediments may have been limited to local migmatization. Bulk chemical compositional variations may have had a role, although the limited data given by Shimron (1972) do not show any significant differences between the compositions of garnet and staurolite schists.

## CONCLUSIONS — IMPLICATIONS OF THE *P–T* DATA

Conditions of 600 ± 25°C → 580°C and 4.6 ± 0.7 → 3.8 kbar have been deduced for a segment of the *P–T* path of the high-grade staurolite-cordierite-$Al_2SiO_5$-zone assemblages of the Elat complex. No spatial variations in the distributions of temperatures were detected. Garnet-zone temperature estimates ranged from 584 to 670°C, greater than expected for pelitic garnet-zone conditions, but possibly consistent with the intrusive relation between the rocks of the zone and the granite gneiss.

Reymer et al. (1984a) and Avigad and Matthews (1985) considered the thermal evolution of the Campus area rocks in terms of a simple regional metamorphic burial. However, the interpretation of temperatures at the contact between the granite gneiss and garnet-zone rocks as possibly representing effects of intrusion also suggests that local heating accompanying igneous intrusion may have had a significant impact on the metamorphic heat configuration. The question of the heat budget will be examined from two aspects: (a) the viability of regional metamorphic heating producing conditions up to staurolite-cordierite-sillimanite grade; (b) the potential significance of high temperatures at the granite gneiss/garnet zone contact for the thermal evolution of the Elat complex.

An approach to the estimation of regional metamorphic conditions can be made by calculating the heat flow needed to sustain rocks at depth of ~15 km and temperatures of ~600°C. To this we have adopted the simple one-dimensional uniform gradient heat flow model used by Reymer et al. (1984b) to analyze conditions in Wadi Kid. Assuming the pelitic rocks were covered by cover consisting of a semi-infinite slab of volcanic rocks of thickness $h$, the heat flux will be given by the equation $q = k/h\ (T_m - T_o)$, where $T_m$ an $T_o$ are metamorphic and surface temperatures, respectively, $q$ the heat flux, and $k$ the heat conductivity. Assuming $T_m$ = 600°C, $T_o$ = 25°C, $h$ = 15 km, and $k$ = 1.5 W $m^{-1}$ $K^{-1}$ (Blackwell et al., 1982) gives $q \cong 60$ mW $m^{-2}$. Using a slightly higher value for "mean" continental crust conductivity of $k$ = 2.25 W $m^{-1}$ $K^{-1}$ (England and Thompson, 1984) gives $q$ = 86 mW $m^{-2}$. Both these calculated values are well within the range of 40 to 100 mW $m^{-2}$ observed by Blackwell et al. (1982) for the active Cascades volcanic region of NW U.S.A. The $q$ value of 86 mW $m^{-2}$ calculated for a mean continental crustal $k$ of 2.25 W $m^{-1}$ $K^{-1}$ is slightly higher than the average continental heat flux of 60 mW $m^{-2}$ given by Sclater et al. (1980).

The calculations above, though of a very simple nature, demonstrate that regional heat flow associated with large-scale magmatic activity is a viable process for the generation of high-grade metamorphic assemblages in the Elat complex. It must be borne in mind that the Elat and Roded associations are largely composed of syn-metamorphic igneous rocks and the association of high-grade metamorphism with regional igneous heat flow is not spurious. The high temperatures apparent in the garnet-zone rocks near their contact with the granite gneiss may further imply that heat was advected into the Campus group of rocks during the intrusion of the granite and contributed locally to the metamorphic heat budget. Similarly, the very high temperatures of around 760°C deduced for Wadi Magrish migmatites also imply the nearby presence of an igneous intrusive heat source. Thus, as a whole, the *P–T* data suggest that the thermal driving force in the metamorphism is a combination of enhanced regional heat flow and heat advected into the complex by igneous intrusion. This conclusion can also be extended to other metamorphic complexes of Sinai, where syn-metamorphic igneous intrusion, andalusite/sillimanite-type metamorphism, and anatectic processes have occurred (e.g., Navon and Reymer, 1984; Reymer, 1985).

## ACKNOWLEDGMENTS

We would like to acknowledge Drs. A. Shimron, Y. Eyal, and M. Eyal for many stimulating discussions on the Elat area. This paper would never have materialized into print without the gentle prodding of Dr. Z. Reiss. Drs. Z. Garfunkel and M. Beyth provided thoughtful reviews of the paper.

## REFERENCES

Amit, O. 1975. The genesis of Wadi Magrish migmatites (NE Sinai), a geochemical investigation. Ph.D. thesis, Hebrew Univ., Jerusalem, 141 p (in Hebrew, English summary).

Amit, O., Eyal, Y. 1976. The genesis of Wadi Magrish migmatites (NE Sinai). Contrib. Mineral. Petrol.

59:95–110.

Avigad, D. 1984. Deformation and metamorphism of schistose dykes in the Elat area, NE Sinai. M.Sc. thesis, Hebrew Univ., Jerusalem, 85 p.

Avigad, D., Matthews, A. 1985. The Elat metamorphic complex revisited. Isr. Geol. Soc. Annu. Mtg., p 164–171.

Bentor, Y.K. 1961. Petrographical outline of the Precambrian in Israel. Bull. Res. Counc. Isr. 10G: 17–64.

Beyth, M., Grunhagen, G., Itamar, A., Zilberfarb, A., Ayalon, A. 1987. The Ataqa metamorphic wedge in southern Sinai. Neues Jahrb. Mineral. Monatsh. 1987: 145–159.

Bielski, M. 1982. Stages in the evolution of the Arabian-Nubian Massif in Sinai. Ph.D. thesis, Hebrew Univ., Jerusalem, 155 p (in Hebrew, English summary).

Blackwell, D.D., Brown, R.G., Hull, D.A., Roccio, J., Steele, J.L. 1982. Heat flow, arc volcanism, and subduction in Northern Oregon. J. Geophys. Res. 78: 8735–8754.

Carmichael, D.M. 1969. On the mechanism of prograde metamorphic reactions in quartz-bearing pelitic rocks. Contrib. Mineral. Petrol. 20:244–269.

England, P.C., Thompson, A.B. 1984. Pressure-temperature—time paths of regional metamorphism. I. Heat transfer during the evolution of regions of thickened continental crust. J. Petrol. 25:894–928.

Eyal, M. 1975. Stages in the magmatic history of the Precambrian in Sinai and southern Negev. Ph.D. thesis, Hebrew Univ., Jerusalem, 155 p (in Hebrew, English summary).

Eyal, Y. 1976. The metamorphic and structural history of the Precambrian massif in Taba Bir-Swair area (northeast Sinai). Ph.D. thesis, Hebrew Univ., Jerusalem, 147 p (in Hebrew, English summary).

Ferry, J.M., Spear, F.S. 1978. Experimental calibration of the partitioning of Fe and Mg between biotite and garnet. Contrib. Mineral. Petrol. 66:113–118.

Garfunkel, Z. 1970. The tectonics of the western margins of the southern Arava. Ph.D. thesis, Hebrew Univ., Jerusalem, 204 p (in Hebrew, English summary).

Garfunkel, Z. 1980. Contribution to the geology of the Precambrian of the Elat area. Isr. J. Earth Sci. 29:25–40.

Halpern, M. 1980. "Pan African" isochron ages of Sinai igneous rocks. Geology 8:48–50.

Halpern, M., Tristan, N. 1981. Geochronology of the Arabian-Nubian Shield in southern Israel and eastern Sinai. J. Geol. 89:639–648.

Holland, T.J.B., Powell, R. 1985. An internally consistent thermodynamic data set with uncertainties and correlations. 2. Data and results. J. Metamorph. Geol. 3:343–370.

Mason, R. 1978. Petrology of the metamorphic rocks. London: George Allen and Unwin, 254 p.

Navon, O., Reymer, A.P.S. 1984. Stratigraphy, structures and metamorphism of Pan-African age in Central Wadi Kid, Southeastern Sinai. Isr. J. Earth Sci. 33:135–149.

Newton, R.C., Haselton, H.T. 1981. Thermodynamics of the garnet-plagioclase-$Al_2SiO_5$-quartz geobarometer. In Newton, R.C., Navrotsky, A., Wood, B.J., eds. Thermodynamics of minerals and melts. New York: Springer-Verlag, 131–147.

Page, M.L. 1972. The geology of the Mt. Shahmon metadiorite complex. M.Sc. thesis, Hebrew Univ., Jerusalem, 99 p.

Powell, R., Holland, T.J.P. 1988. An internally consistent data set with uncertainties and correlations. 3. Application to geochemistry, worked examples and a computer program. J. Metamorph. Geol. 6:173–205.

Reymer, A.P.S. 1983. Metamorphism and tectonics of a Pan-African terrain in southeast Sinai. Precambrian Res. 19:225–238.

Reymer, A.P.S. 1985. The origin and microstructures of metamorphic felsic dykes emplaced during brittle-ductile extension, Southeast Sinai. Geol. Mag. 122:27–38.

Reymer, A.P.S., Matthews, A., Avigad, D. 1984a. Inverse metamorphic zonation, thrusting and folding in Arabian Shield in N.E. Sinai: Evidence for Pan African crustal shortening. Geol. Soc. Am. Abstr. with Progr. 16:633 (abstract).

Reymer, A.P.S., Matthews, A., Navon, O. 1984b. Pressure-temperature conditions in the Wadi Kid metamorphic complex: Implications for the Pan-African event in SE Sinai. Contrib. Mineral. Petrol. 85:336–345.

Sclater, J.G., Jaupart, C., Galson, D. 1980. Heat flow through oceanic and continental crust, and heat loss of the Earth. Rev. Geophys. Space. Phys. 81:269–312.

Shimron, A.E. 1972. The Precambrian, structural and metamorphic history of the Elat area, with comparative notes on the metamorphic rocks of the Sinai peninsula. Ph.D. thesis, Hebrew Univ., Jerusalem, 244 p.

Shimron, A.E. 1980. Proterozoic island arc volcanism and sedimentation in Sinai. Precambrian Res. 12:437–458.

Shimron, A.. 1987. Pan-African metamorphism and deformation in the Wadi Kid Region, SE Sinai Peninsula: Evidence from porphyroblasts in the Umm Zariq Formation. Isr. J. Earth Sci. 36: 173–193.

Thompson, A.B. 1982. Dehydration melting of pelitic rocks and the generation of $H_2O$ undersaturated granitic liquid. Am. J. Sci. 282:1567–1595.